UNIVERSITY OF AMSTERDAM

UvA-DARE (Digital Academic Repository)

A study on giant radio pulses

Karuppusamy, R.

Citation for published version (APA):
Karuppusamy, R. (2009). A study on giant radio pulses

Download date: 21 Jul 2018

A Low Frequency Study of PSRs B1133+16, B1112+50, B0031−07 and J1752+2359

R. Karuppusamy, B. W. Stappers and M. Serylak

Abstract   We use the low frequency capabilities of the Westerbork synthesis Radio Telescope (WSRT) to characterise a large collection of single pulses from four low magnetic field pulsars by means of pulse energy and intensity distributions, microstructure and drifting subpulse analysis. The study examines the presence of giant pulse emission in these pulsars using the Pulsar Machine II (PuMa-II) to acquire and coherently dedisperse the signals from the pulsars. Classical giant pulses are reported from PSR B1112+50 and very bright pulses in PSRs B1133+16 and B0031−07. All three pulsars show a large modulation that points to rapid changes in the single pulse intensity. Evidence for global magnetospheric effects are provided by our detection of bright double pulses. Using multi frequency observations, emission heights in PSR B1133+16 are estimated. We report our non-detection of giant pulse radio emission from the PSR J1752+2359. We have accurately estimated the dispersion measure of two pulsars and report on the subpulse drift modes in these pulsars.

4.1   Introduction

Most radio pulsars are characterised by a stable average pulse profile at a given sky frequency. The average profiles are formed by integrating all pulses emitted by the star over a given time. The pulsed emission from the star is observed as individual pulses and they carry detailed information on the physics of the pulsar radio emission. These pulses can be directly detected in a less than a third of the known radio pulsars, mainly due to their weak nature. One of the remarkable features in the single pulse emission is the occurance of intense pulses called giant pulses which are defined as pulses with energy greater than 10 times the average pulse energy. Furthermore, the giant pulses are very narrow when compared to the width of average pulsed emssion and result in a pulse intensity distribution described by a power-law. For example, in the radio emission of the young Crab pulsar, the width of the giant pulses are found to be less than 0.4 ns wide implying a large brightness temperature of $\sim 10^{41}$ K (Hankins & Eilek 2007) and the single pulse flux distribution follows a power-law with slope -3.3 (Lundgren et al. 1995). Another example is the emission of single bright pulses from the young Crab-like pulsar, B0540$-$69 in the Large Magellanic Cloud; the pulsar is visible at radio wavelengths only by virtue of the star's intense giant pulse emission (Johnston & Romani 2003). Similar bright and narrow pulses were reported in the emission of the very old millisecond pulsars like PSR B1937+21 (Cognard et al. 1996) and B1821-24 (Romani & Johnston 2001). Concerted giant pulse searches in these older and short period pulsars have revealed more giant pulse sources eg. PSRs J1823-3021A and J0218+4232 (Knight et al. 2005, 2006b). The only common feature in these pulsars is the large magnetic field ($B_{LC} \sim 10^5$ G) at the velocity of light cylinder which is the limiting radius where the co-rotation of plasma and magnetic field lines have a velocity less than the speed of light.

However, some recent studies propose giant pulse like emission in pulsars with a low magnetic field at the light cylinder e.g $B_{LC} \sim 4$–100 G. For instance, the bright single pulse emission from PSRs B0031$-$07, J1752+2359 and B1112+50 at 40 and 111 MHz (Kuzmin & Ershov 2004; Ershov & Kuzmin 2005, 2003). Similarly, Kramer et al. (2003) report bright pulses from PSR B1133+16 at 5 GHz. If these bright pulses are similar to the classical giant pulses, this questions the requirement of a large value of B_{LC} to produce giant radio emission. After the initial discovery studies of the bright pulses in these low B_{LC} pulsars, a detailed statisical analysis has not been attempted, unlike the extensive studies on the giant pulses from the young pulsars and the millisecond pulsars (Lundgren et al. 1995; Kinkhabwala & Thorsett 2000; Knight 2007; Knight et al. 2006a).

The pulsars in this study show other interesting single pulse behaviour: PSRs B1133+16, B0031$-$07 and B1112+50 show drifting subpulses (Backer 1973; Taylor et al. 1975; Wright et al. 1986) and nulling (Herfindal & Rankin 2007; Ritchings 1976; Wright et al. 1986; Vivekanand 1995). PSR B1133+16 also shows narrow emission features called microstructure (Hankins 1972; Cordes et al. 1990; Lange et al. 1998). Among the pulsars studied in this work, PSR J1752+2359 appears to be unique in that the pulsar spends about 70-80% of the time showing no detectable radio emission (Lewandowski et al. 2004); the emission when resumed, occurs in bursts that last a few stellar rotations before exponentially decaying to an off-state over the next few pulse periods.

Radio pulsars in general show a negative spectrum (Slee et al. 1986) and a low frequency spectral turnover (Kuzmin et al. 1978; Malofeev et al. 1994). This implies that pulsars are brighter at low sky frequencies although the sky temperature also increases, contributing significantly to the background. Moreover, microstrucure and drifting subpulses are better studied at low frequencies when sufficient telescope sensitivity is available (Cordes et al. 1990). Motivated by the possible presence giant pulses, and a rich single pulse behaviour and the availability of the Low Frequency Front Ends (LFFEs) at the WSRT we undertook this study in the 115–180 MHz frequency range. The flexible baseband recorder PuMa-II described in Chapter 2 and full coherent dedisperion, permitted a detailed single pulse study with high sensitivity and relatively high time resolution. Although these pulsars have been studied at low sky frequencies before, with our system we are able to observe much longer and with much larger frequency coverage. Our long observations are useful in determining the flux distribution and the occurance rates of bright pulses. Furthermore, the large frequency coverage permits the computation of the pulsar spectra in this band.

The rest of this chapter is organised as follows: the observations and the estimation pulsar fluxes and spectra are described in §§ 4.2 and 4.3. We present our revised values of the dispersion measure (DM) of two pulsars based on the narrow giant pulses in § 4.5. The single pulse intensity, energy distributions and microstructure are the subjects of discussion in § 4.6. We proceed with the pulse drift analysis in § 4.8 followed by discussion and conclusions.

4.2   Observations and data reduction

Pulsar	Date	Duration	N_{pulses}
J1752+2359 . . .	16 Jun 2008	718 min.	∼104700
B1133+16	23 Nov 2008	280 min.	∼13701
B0031−07	02 Nov 2008	360 min.	∼22758
B1112+50	01 Oct 2008	570 min.	14286

Table 4.1: Observation details for the four pulsars.

The pulsars were observed with the Westerbork Synthesis Radio Telescope (WSRT) on four different days between June and November 2008 (see Table 4.1) using the Low Frequency Front Ends (LFFEs) that can be tuned to any frequency in the 115–180 MHz part of the radio spectrum. The design of the WSRT backend receiver system allows the selection of a maximum of eight different radio bands within the frequency range of the front end receiver. Eight 2.5 MHz-wide bands tuned to 116.75, 130, 139.75, 142.25, 147.5, 156, 163.5 and 173.75 MHz sky frequencies were used for these observations. These bands also showed comparatively little radio frequency interference (RFI). The bands were recorded and processed using the PuMa-II instrument. When possible, the observations were carried out in the early hours of the day, reducing the effect of RFI. Despite our careful choice of the frequency bands and observing times, some factors that made these observations susceptible to

RFI were: strong in-band RFI in the passband of the LFFE electronic amplifiers; the presence of the automatic gain control (AGC) in the WSRT's signal chain and the 2-bit system design. Therefore, the data were subjected to an extensive RFI cleaning procedure by a combination of automated algorithms and visual examination.

The WSRT was operated in the tied-array mode by adding signals from 13 telescopes each of 25–m diameter. The analogue signals from the individual telescopes were digitally sampled at 2-bit resolution and a fixed rate of 40 MHz. The 2-bit data were then coherently added in a dedicated hardware unit to produce the 6-bit tied-array data. Coherent addition improves the signal-to-noise (S/N) ratio by a factor 13, while reducing the array's field of view. The summed data was then read into PuMa-II as 8-bit numbers, downsampled by a factor of 8 in realtime and written to disk. Single pulses were generated from the coherently dedispersed baseband data using the dispersion measure in the catalog and based on a polynomial determined by the TEMPO software (Taylor & Weisberg 1989). The open-source software DSPSR[1] was used to form a 64-channel software filterbank across the 2.5 MHz bands and the pulsar signal was coherently dedispersed in every channel. The resulting frequency–time cubes were written to the disk as single pulses. The original time resolution of 2.5 μs and the formation of a 64-channel synthetic filterbank permitted 2048 samples across the pulse period of the four pulsars observed and the final time resolutions are in column 4 of Table 4.2. The large number of frequency channels was used later to correct for the residual dispersion smearing, as the DMs in the catalog had either changed or were not sufficiently accurate and it also aided the removal of narrow band RFI in the signal. Extensive use of the PSRCHIVE package (Hotan et al. 2004) was made in the computation of the total intensity, signal-to-noise ratio and visual inspection of the single pulses for RFI. Pulse stacks were formed by stacking individual pulse intensitites one above the other according to their phases. When required, the signal was flux calibrated using the off-pulse radiometer noise. With the computed fluxes in each band, various statistical analysis of the data was performed.

4.3   Low frequency flux

4.3.1   Radio frequency interference

The data was cleaned of interference using various cleaning strategies for the three purposes: estimation of mean flux density, fluctuation analysis and single pulse flux estimates. For the mean pulse flux computation, the pulses that showed excessive noise, negative drop outs and large intensity peaks in the off-pulse region were removed. The single pulses were then combined to create pulse stacks which were examined for the second time as time–phase plots; pulses that were missed by the automated algorithm were now identified and removed. The remaining pulses were then averaged over the period of integration to compute the average pulse profile. The number of pulses removed in this method was accounted for in the time term of equation 4.1 before the profile was flux calibrated. From the calibrated profiles the spectral indicies were derived.

---

[1]http://dspsr.sourceforge.net/

For the fluctuation analysis the pulses were first gated to contain at least three times the width of the average pulse profile at the lowest observed frequency. The gated pulse stack was then subjected to the two-pass RFI cleaning procedure explained above. Pulse stacks were inspected by eye and pulses that showed a saturation in the off-pulse phases were now replaced by zeros. This procedure was repeated until a visually clean image is seen in the time–phase plane.

The single pulse statistics were computed based on only the bright single pulses in the eight bands observed. RFI was cleaned from the dedispersed single pulses by visually examining the frequency–phase images within $30°$ of the pulse longitude. For these comparatively long period pulsars, retaining a narrow phase range of the pulse period has the advantage of being less sensitive to impulsive RFI affecting other pulse longitudes. Only pulses that showed the required dispersion were retained. An interactive plot utility was developed to examine the frequency–phase images of the large S/N pulses.

4.3.2 Flux Calibration

Calibrating pulsar fluxes at low sky frequencies at the WSRT is difficult for three reasons: First the main contribution to the system noise T_{sys} is from the sky temperature, T_{sky}, which depends on the position of the pulsar on the sky. Second, the aperture efficiency of the LFFE's at the WSRT is poorly constrained and thirdly, the presence of RFI introduces errors in flux measurements of the calibrators and the pulsars. The system parameters (telescope gain and system tempertaure) were derived based on continuum observations of the calibrator source 3C196 made shortly before these measurements. From these measurements, the aperture efficiency is estimated to be ~30% translating to an effective telescope collecting area of 1500 m^2. A constant value T_{sys} in the entire 115–180 MHz is used, since the Galactic synchrotron foreground varying with frequency as $v^{-2.6}$ is offset by the frequency dependent amplitude gains of the LFFEs. The system temperatures derived in this manner are shown in Table. 4.2. Assuming a frequency scaling of $v^{-2.6}$, the sky temperature estimated from the 408 MHz continuum maps of Haslam et al. (1981) in the direction of these pulsars are consistent within 20% of the system temperatures listed in Table 4.2. The large sky temperature in the direction of PSR J1752+2359 rendered the pulsar undetectable in our obervations.

Pulsar	T_{sys} (K)	N_{bins}	τ (μs)	S_{min} (Jy)
B1112+50	400	2048	809	9.0
J1752+2359	600	1024	400	19.3
B1133+16	400	2048	580	10.7
B0031−07	400	2048	460	12.0

Table 4.2: Telescope parameters and observation details for the four pulsars observed. The minimum detectable signal per time sample is based on a 30% aperture efficiency.

Once the telescope gain and system temperature were established, the off-pulse noise in flux units was computed using the radiometer equation (Lorimer, D. R. and Kramer, M.

2005),

$$S_{av} = \frac{S_{sys}}{\sqrt{N_p \cdot B \cdot T_{int}}} , \qquad (4.1)$$

where $S_{sys} = T_{sys}/G$ is the system equivalent flux density in Jy, N_p is the number of polarizations summed, and T_{int} is the equivalent integration time. The pulse profile is then flux calibrated by multiplying by S_{av}. Now, integrating the fluxes in all phase bins and dividing by the total number of bins gives the mean continuum flux density of the pulsar. While this method is not as accurate as the absolute flux measurements based on noise generators, this is the only option in a synthesis telescope like the WSRT for non-imaging observations; it also yields fluxes comparable to those reported elsewhere.

In our method of detecting the pulsars, the dedispersed signal was written to the disk as single pulses. Following the formation of total intensities, diagnostic plots of peak S/N against the phase of the peaks were made. Any pulsed emission now show as bunching of data points near the nominal emission phase and the corresponding pulses were visually examined. Combining the single pulses in time after removing the RFI afflicted pulses produced the average emission profiles. Thus, this method is sensitive to any pulsed emission above the noise floor. We fail to detect any significant emission from PSR J1752+2359 in either single pulse or averaged pulse emission and it is due to the large system temperature. As evident from Table 4.2, the system temperature for PSR J1752+2359 is 1.5 times the corresponding value for the other three pulsars due to its location near the Northern Polar Spur (see Table 4.2). Based on the flux of 3.5 mJy (Lewandowski et al. 2004) at 400 MHz, this pulsar has a mean flux density of only ∼14 mJy at 116 MHz, if a nominal spectral index of −2 is considered. Moreover, from the work of Ershov & Kuzmin (2005), the pulse energy distribution has a slope of $\alpha = -3.0 \pm 0.4$. With our system, this implies that a pulse $\geq 10\sigma$ will need an observation length of at least 12 hours. Therefore, the non-detection of the average and single pulse emission from PSR J1752+2359 is due to our limited system sensitivity and the low occurance rates of bright pulses in this pulsar. Hence this pulsar will not considered in the rest of this chapter.

4.3.3   Profile evolution

The average pulse profiles in all recorded bands for the three detected pulsars are displayed in Figure 4.1. The characteristic age of PSR B1112+50 is 10 Myr, and shows 10% peak widths $W_{10} = 35.5$–38.8 ms in this frequency range. This can be compared to $W_{10} = 35.0$ ms at 405 MHz (Lorimer et al. 1995). The single component in the average emission of PSR B1112+50 at these frequencies and at 328 MHz (Weltevrede et al. 2006a) evolves to a two-componenent average emission profile at 1400 MHz (Wright et al. 1986).

PSR B0031−07 with a characteristic age of 36 Myr shows $W_{10} = 120.2$–155.1 ms, while Lorimer et al. (1995) report a value of 104.5 ms at 405 MHz. The trailing edge in the average profile of PSR B0031−07 shows a gradual decrease in steepness with frequency and this is not due to scattering in the ISM. This was confirmed by visual inspection of several single pulses which show no strong evidence for scatter broadening. However, this change in slope
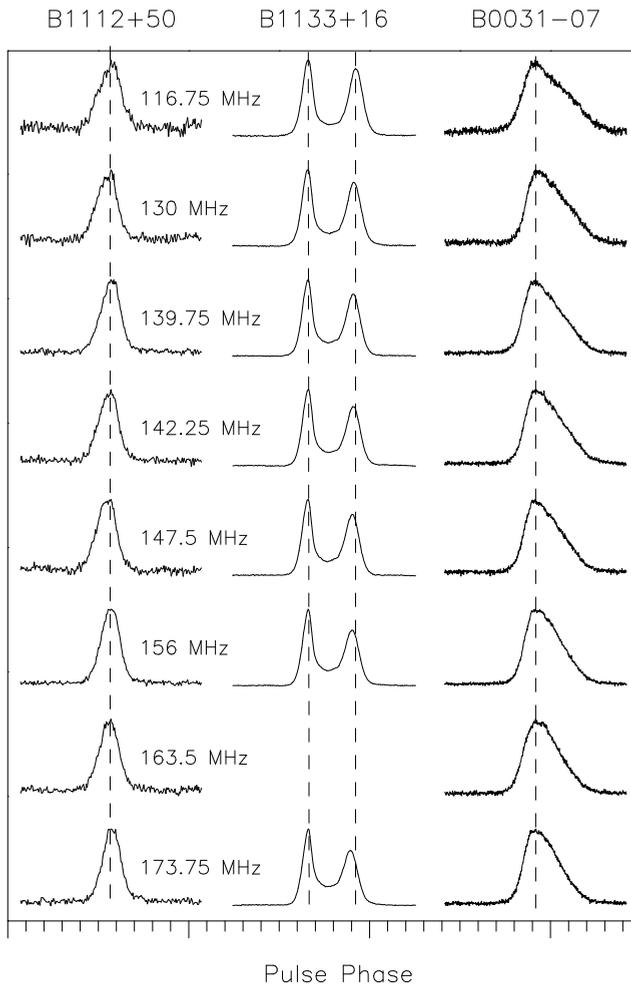
Figure 4.1: Average pulse profiles of the three pulsars. The profile changes with sky frequency is clearly evident. The profile for PSR B1133+16 at 163.5 MHz is not shown, as it was too corrupted by RFI. The profiles correspond to 0.098, 0.15 and 0.34 stellar rotations of PSRs B1112+50, B1133+16 and B0031−07 respectively. All profiles are normalized by the maximum flux density in the band and are aligned at the phase of maximum intensity in each band. Profiles at 116.75 and 130 MHz have comparatively more noise, as up to 15% of pulses were removed due to RFI which reduced the effective integration time.

is indicative of the emergence of a second emission component at even lower frequencies e.g at 40 and 62 MHz (Izvekova et al. 1993), which is quite the opposite behaviour of the average emission profile in PSR B1112+50. Another contribution to the slope of the trailing part of the average emission profile in PSR B0031−07 could be the vertically drifting subpulses

seen in this pulsar as discussed in §4.8. The general expectation of a narrower pulse profile for older pulsars is not valid with respect to these two pulsars, as the impact angle of the observer's line of sight with the emission beams from the pulsars may not be equal.

PSR B1133+16 shows a profile width of W_{10} = 44.0–48.1 ms compared to 41.8 ms at 405 MHz (Lorimer et al. 1995). The component separation of the average profile decreases with frequency and this phenomenon was successfully explained by the radius-to-frequency mapping in the pulsar magnetosphere (Cordes 1978). The average profile also shows a double emission component, with a pronounced bridge emission that rises from 14% to 25% of the peak flux density at our lowest and highest frequencies, respectively. Similarly, the second component in the average emission profile reduces from 90% to 70% of the leading component intensity with increasing frequency. Clearly, these variations probe different parts of the emission beam. Nowakowski (1996) assumed a model in which the pulsar beam consists of two concentric emission cones to explain the observed two-component emission profile and the increasing bridge emission with frequency. However, this model is unable to explain why multiple emission components are not visible at higher frequencies. Polarisation observations of this pulsar over a range of frequencies would offer further insights in to the emission geometry. As discussed later in this work and by Kardashev et al. (1982), the emission height of various radio frequencies in the magnetosphere of the pulsar can be derived using the frequency dependence of the component separation. Our analysis shows that a $\nu^{-0.30\pm0.02}$ scaling law holds for the component separation in the frequency range considered here and is consistent with $\nu^{-0.24}$ and $\nu^{-0.26}$ scaling laws derived by Backer (1972) and Sieber et al. (1975), respectively.

4.3.4 Radio Spectrum

The observations here span a reasonably large frequency range and we use the flux of the pulsar in each of the bands observed to compute the pulsar spectra. The flux of the pulsar used here is the mean continuum flux density of these sources, computed from the flux calibrated pulse profiles. The functional form of the radio spectrum of the pulsars was assumed to follow $S(\nu) \propto \nu^{\alpha}$, where $S(\nu)$ is the pulsar flux at frequency ν and α is the spectral index. The parameter α was estimated using a least squares fitting procedure and the result is displayed in Figure 4.2 and Table 4.3 for the three pulsars. To account for the effect of RFI and possible errors in telescope parameters, a 10% uncertainty in the estimation of the pulsar flux density in each band is considered which dominates other errors in signal-to-noise ratio estimations as all pulsars are strongly dectected.

PSR B1112+50 shows a slightly positive spectral index and we find a value of $\alpha = 1.12 \pm 0.46$. Even though this pulsar is the weaker of the three pulsars considered in this section, it is detected with high significance, as evident from Figure 4.1. Low DM pulsars, as in this study, are usually in the strong scintillation regime at sky frequencies less than 1 GHz and this was confirmed for PSR B1112+50 as follows. On visual inspection of several single bright pulses detected in seven bands, the spectral modulation was always limited to 3–4 channels. This is less than 10% of the 64 channels in each band. Considering an upper limit of 10% of the bandwidth, the diffractive scintillation bandwidth $\Delta\nu_{DISS}$ is $\leq$ 250 KHz. Since $\Delta\nu_{DISS}$ is
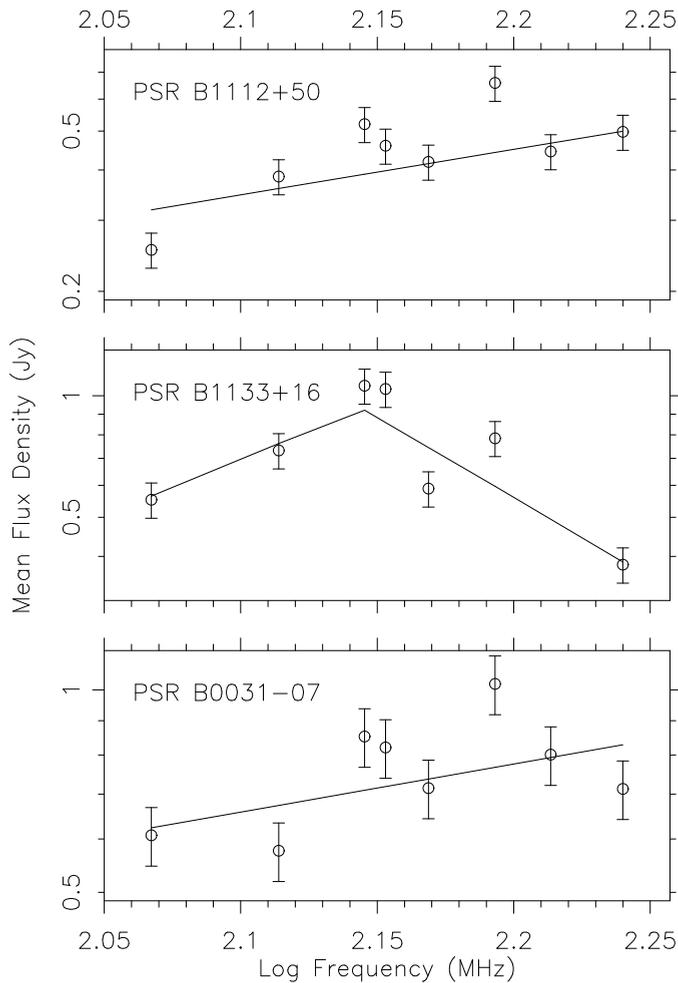
Figure 4.2: Spectra for three pulsars in the frequency range 100–200 MHz. Errors bars are correspond to 10% uncertainty in the pulsar flux estimation. The best fit power law curves are also displayed. For PSR B1133+16, a broken power-law results in a better fit to the measured fluxes. The flux in the RFI affected band centred at 163.5 MHz is not included for PSR B1133+16.

much less than the receiver bandwidth, scintillation cannot be a possible cause for the scatter in the measured fluxes and the variations in intensity are more likely an underestimatation of the errors. Therefore the poor fit to the pulsar spectra in the band observed is not caused by fluxes corrugated by scintillation.

For PSR B1133+16, the middle panel of Figure 4.2 can be compared to Figure 4e in Deshpande & Radhakrishnan (1992) that extends down to 34.5 MHz. Their figure can be interpreted as indicating a spectral turnover in our frequency range. With this consideration,

Pulsar	S (mJy)	α_1	α_2
J1752+2359	< 2.08	-	-
B1112+50	460±46	1.12±0.56	-
B1133+16	1030±51	2.33±2.55	-3.81±2.24
B0031−07	821±41	0.71±0.45	-

Table 4.3: Measured flux density and spectral index of the three pulsars are shown in columns 3 and 4. The flux density quoted here is the value measured at 142.25 MHz. For PSR J1752+2359, the upper limit quoted is based on a 3σ detection threshold in a 12 hour–integration. For PSR B1133+16 a broken power-law spectrum results in a better fit.

the spectrum was modelled by a two component power-law defined as,

$$S(v) = \begin{cases} C_1 v^{\alpha_1} & \text{if } v < v_b \\ C_2 v^{\alpha_2} & \text{if } v \geq v_b. \end{cases} \quad (4.2)$$

where, v_b is the break frequency, C_1 is a constant and normalisation yields $C_2 = C_1 v_b^{\alpha_1 - \alpha_2}$. The values of break frequency of 139.75 MHz with spectral indicies $\alpha_1 = 2.33 \pm 2.55$ and $\alpha_2 = -3.81 \pm 2.24$ were derived from the best fits to the data. As with PSR B1112+50, we confirm that scintillation has no effect on the spectral index derived here. As a further confirmation, the scintillation bandwidth and timescales at this sky frequency were computed using $\Delta v_{DISS} \propto v^{4.4}$ and $\Delta t_{DISS} \propto v^{1.2}$ scaling laws and the values listed in Kramer et al. (2003). These "scintiles" with typical widths of ≤ 40 KHz average out within each 2.5 MHz band and do not contribute to the intensity variations in the 115-180 MHz frequency range. Combined with the 75% error on 400 mJy at 151 MHz (Sieber 1973) and 900 mJy at 111 MHz (Figure 3; Malofeev et al. 1994), we conclude that our results are consistent with those reported previously.

We find a relatively flat spectrum for PSR B0031−07 with an index of $\alpha = 0.71 \pm 0.45$. As for the other two pulsars, B0031−07 has partially resolved scintillation (see Figure 4.3) at these frequencies that do not contribute to the estimated fluxes. In the work of Malofeev et al. (1994), they show that the spectral index of this pulsar is $\alpha = -1.2 \pm 0.26$ for $v \leq 1$ GHz. Excluding the two points near ~100 MHz in Figure 2 of their work, the data is indicative of low frequency turn at ~200 MHz. Considering this and the errors bars in the low frequency fluxes in Malofeev et al. (1994) the spectral index we derive here is consistent with the former work.

4.4   Bright single pulses

Several bright pulses were detected from all three pulsars and one example from each pulsar is shown in Figure 4.3. These pulses are very narrow, restricted to less than 1 ms. Normally, giant pulses are characterised by their widths, the phase of the pulses with respect to the average emission profile and the pulse energy (Knight 2007). The classical giant pulses are

also found to be broad band, for example in B1937+21 $\Delta\nu/\nu \sim 0.2$ (Popov & Stappers 2003), where ν and $\Delta\nu$ are the observation frequency and bandwidth. In this study, we find similar bright, broad band bursts from these pulsars, although they are not as energetic as the classical giant pulse emitters.
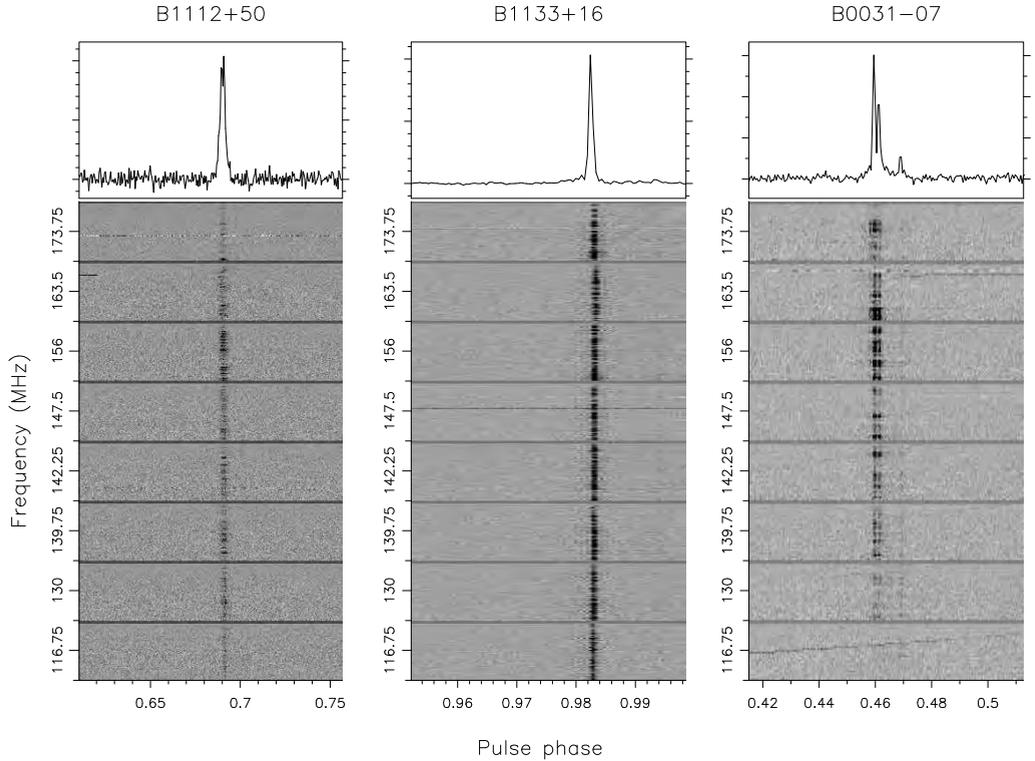

Figure 4.3: Narrow bright pulses from the three pulsars detected at all eight sky frequencies. The total intensity displayed in the top panels is computed by summing the signal in the 8 bands. The lower panels show a dedispersed pulse as a frequency–phase plot. Some residual RFI is visible as low-level intensity modulating across the entire pulse phase in the frequency-phase plots of all three pulsars.

The implied brightness temperature of the single pulses can be computed from (pp. 79; Lorimer, D. R. and Kramer, M. 2005),

$$T_B = \left(\frac{S_{peak}}{2\pi k_B}\right)\left(\frac{\nu\Delta t}{d}\right)^{-2},\qquad(4.3)$$

where S_{peak} is the peak pulse flux, k_B is the Boltzmann's constant, d is the distance to the pulsar, ν the sky frequency and Δt is the pulse width. At 156 MHz, using Δt values from Table 4.2, and the known pulsar distances[2] (Taylor & Cordes 1993), the brightness temperatures for

---

[2]values are from http://www.atnf.csiro.au/research/pulsar/psrcat/

the pulses displayed in Figure 4.3 are 3.5×10^{26} K, 3.6×10^{27} K and 2.6×10^{27} K for PSRs B1112+50, B0031−07 and B1133+16, respectively. The large brightness temperatures point to a coherent emission mechanism for these pulses. From the frequency–phase plots in Figure 4.3, clearly these bright pulses are broad-band emission, with $\Delta\nu/\nu = 0.3$, and can be compared to the value of 0.1 and 0.2 for the Crab pulsar and PSR B1937+21 at 1400 MHz. Also visible in this figure are the scintiles in all three pulsars, though it is more evident in PSRs B1133+16 and B0031−07.

4.5 DM Changes

Pulsar dispersion measures are normally estimated from the multi-frequency multi epoch timing observations (Phillips & Wolszczan 1992; Backer et al. 1993). However, in some pulsars the absence of an appropriate fiducial point on the average emission profile introduces errors in the estimated DM values. Ahuja et al. (2005) used cross correlation of the pulse profiles at two different frequencies of observation to partially overcome this problem. As pointed out by these workers, an alternative to estimate the DM is to use multi-frequency simultaneous observation of the pulsar, and use a fiducial point in the average emission profile to align the profiles at the two frequencies. Our detection of single, narrow and bright pulses at low sky frequencies results in an excellent reference to align the pulses and hence compute the DM very accurately for these low DM pulsars. The frequency resolution of 64 channels across each 2.5 MHz band gives a total of 512 channels in the 115–180 MHz range which permits the accurate determination of the quadratic dispersion curve. We generally started with the catalog DM's and the DM value was varied until a peak S/N in the combined pulse profile is attained. The frequency-phase plots were then visually inspected for the pulse alignment using the new value of DM. To compute the change in the DM at the epoch of our observations, the dispersion smearing due to the use of an incorrect DM within a single frequency channel is considered negligible.

From their multi-year timing data, Hobbs et al. (2004) found for PSR B1133+16, a DM = 4.864 pc cm^{-3} corresponding to epoch MJD 46407 and they also determine $|\mathrm{d(DM)}/\mathrm{d}t| \approx -0.0008$ pc cm^3 yr^{-1}. Our analysis shows that the DM has changed to 4.844±0.002 at epoch MJD 54793 from our reference DM of 4.871 at epoch MJD 41665. The error estimate is computed from the DM uncertainty incurred in the misalignment of a broadband pulse by one phase bin across the 115–180 MHz band. The total change in DM, ΔDM found here is consistent with the predictions of Hobbs et al. (2004). The somewhat large yearly rate of change in the DM of this pulsar probably arises from its large proper motion ~ 630 km s^{-1}. The ΔDM = 0.0265 corresponds to 0.5% change in DM and not correcting for this change results in the peak flux of the bright pulses being underestimated by ∼3%.

For PSR B1112+50, we find that the DM increased from 9.16 at an epoch MJD 50899 to 9.175±0.0001 at epoch of MJD 54795. From this, the total DM change, ΔDM is 0.015 pc cm^{-3}. The error in our DM values are derived from pulse misalignment by one phase bin in a 2.5 MHz band at 147.5 MHz. We again refer to Hobbs et al. (2004) for DM estimates for this pulsar, where they find DM = 9.195 and a yearly DM rate, $|\mathrm{d}DM/\mathrm{d}t| = -0.004$ cm^{-3} pc yr^{-1}. These values are inconsistent with the rate of -0.0014 cm^{-3} pc yr^{-1} derived from

our analysis. One reason for this discrepancy could be the high frequency observations at 408–1600 MHz used in the work of Hobbs et al. (2004) compared to our study at much lower frequencies which is more sensitive to DM changes. The second reason could be that a single value for $|\mathrm{d}DM/\mathrm{d}t|$ is insufficient implying higher order terms of the DM time derivative may be necessary to accurately model the DM variations.

We do not detect a change in the DM of PSR B0031−07 from the reference DM value of 10.89. The narrow and bright single pulses align with no visible errors when the signal is dedispersed with this DM. However, the pulsar's DM of 10.89 is inconsistent with the value of 11.29 at this epoch expected from the −0.007 cm^{-3} pc yr^{-1} listed in Hobbs et al. (2004). This argues that the DM value and the rate for this pulsar in their work is incorrect. Furthermore, earlier work by Taylor et al. (1993); Kuzmin & Ershov (2004) and Smits et al. (2007) have made use of a DM = 10.89 consistent with no change in the DM of the pulsar.

4.6 Single Pulse Analyses

Our long observations resulted in the detection of a large number of pulses, as shown in Table 4.1. Robust statistics can be obtained by computing the distribution of single pulse energies E and peak intensities S_p. A scatter plot of the peak fluxes and the average emission profile for the three pulsars are shown in Figure 4.4. The 2.5 MHz band at 156 MHz was chosen out of the eight bands for further study because it showed comparatively less RFI. We note that after an exhaustive RFI search and removal, all eight bands show similar trends.

The presence of narrow bright pulses was evident when the data was examined visually in the RFI cleaning stage. Such unusal emission entities would be evident in the single pulse energy and flux distributions. For example, giant pulses in the emission of the Crab pulsar results in a power-law in the pulse flux distribution (Lundgren et al. 1995). For the three pulsars considered here, the distribution of the pulse flux and energy are shown in Figures 4.5 and 4.6, respectively. The pulse energy was computed by summing the emission in a window of width equal to the average emission profile. The single pulse peak flux was computed as the product of the peak S/N and S_{av} (equation 4.1).

4.6.1 PSR B1112+50

Giant pulse like emission from this pulsar was reported by Ershov & Kuzmin (2003). The bright pulses occur in the middle of the average pulse profile, but a slight preference to the trailing edge is seen (Figure 4.4; top panel). These pulses are also seen in the pulse energy distributions as those with energies greater than $10 \times \langle E \rangle$ in Figure 4.5. An indication of the null emission in this pulsar is visible from the slight turn over in the pulse energy distribution near $3 \times \langle E \rangle$ which is similar to the offpulse energy distribution. While this pulsar shows $\geq 60\%$ nulling fraction at 1412 MHz (Wright et al. 1986), with our system sensitivity the nulling fraction cannot be ascertained. The pulse flux distribution also displays a shallow power-law like tail in the peak flux distribution (Figure 4.6; top panel) which is due to the occassional bright pulses in this pulsar.
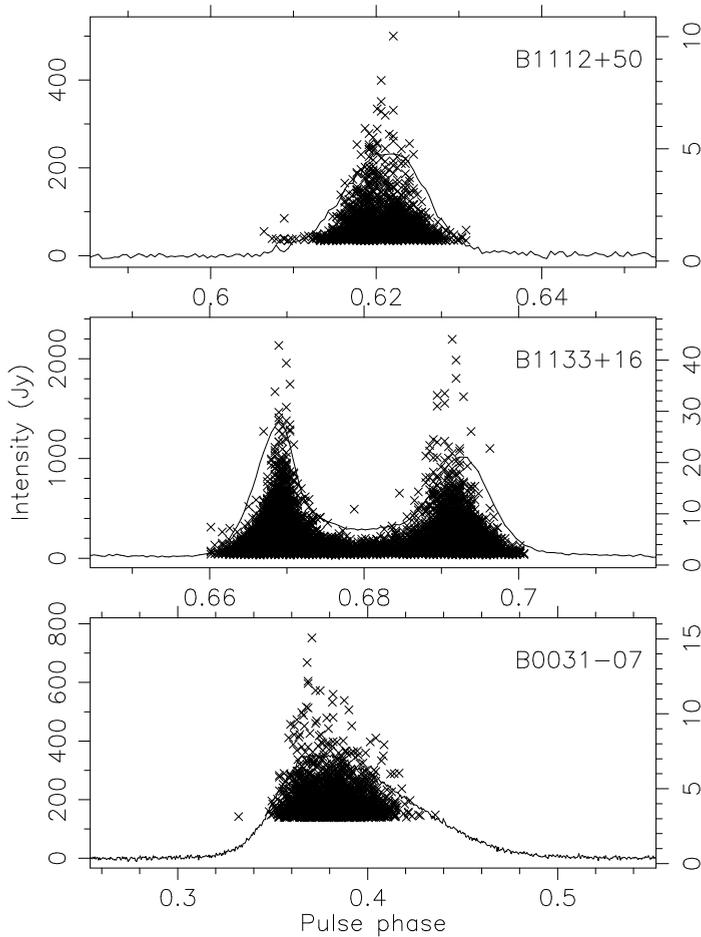
Figure 4.4: Single bright pulses and the integrated pulse profiles at 156 MHz for the three pulsars. The flux scale on the left ordinate corresponds to the peak flux of the single pulses and the scale on the left ordinate axis corresponds to the average pulse profile. Peak flux densities of the single pulses are shown. Only single pulses $\geq 20\sigma$ are shown in these plots and results in the low flux cut-off in the fluxes of single pulses.

4.6.2   PSR B1133+16

Kramer et al. (2003) reported bright pulses from this pulsar at a frequency of 5 GHz but not at 1.4 GHz. We detected bright and narrow pulses in all eight bands in the range 115-180 MHz with peak fluxes larger than 10 times the peak of average flux density (Figure 4.6; middle panel). However, the pulse energy distribution (Figure 4.5; middle panel) can be qualitatively approximated by power-law and does not show pulses with energies $>10 \times \langle E \rangle$,
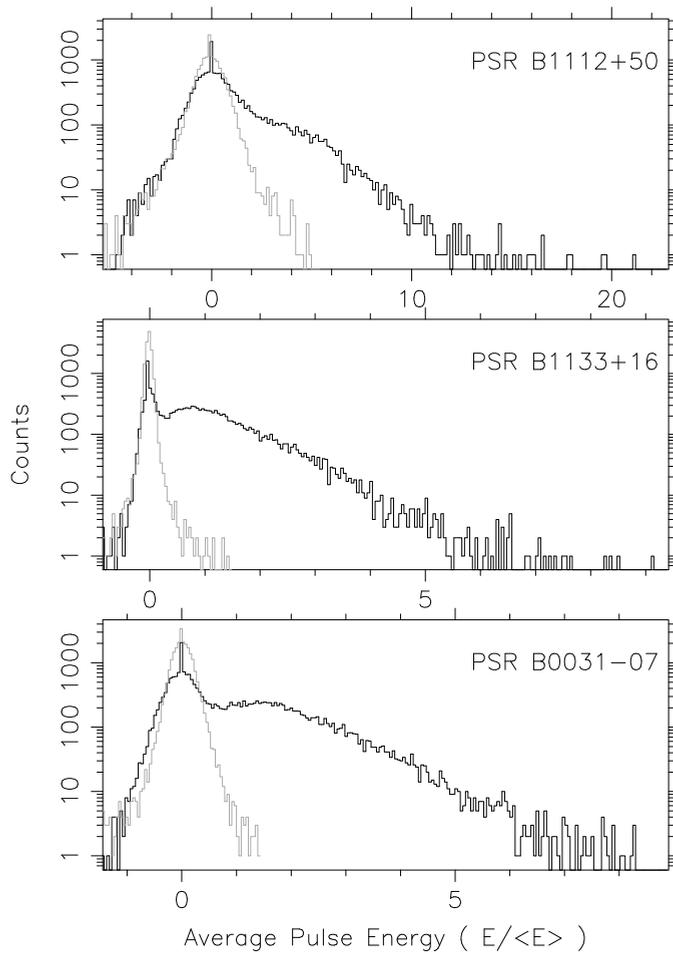
Figure 4.5: Distribution of the single pulse energies for three pulsars. The abscissae show the pulse energy normalized to the mean pulse energy. Dark and light grey lines correspond to the on-pulse and off-pulse energy distributions. The clear peak at zero energy is introduced by the RFI affected pulses replaced by zeros.

which is the normal working definition of giant pulses (Cognard et al. 1996). From the middle panel in Figure 4.4, a preference for the bright pulses to fall on the inner edge of the two components is evident. Such bright pulses at 327 MHz were also noted by Herfindal & Rankin (2007). The turn over in the pulse energy distribution $\sim 1.0 \langle E \rangle$ points to the presence of a bimodal distribution, strongly suggesting the presence of nulling. The pulsar shows $\sim 20\%$ null fraction at 327 MHz (Herfindal & Rankin 2007), but at our frequency we are unable to discrimnate the null distribution definitively due to the limited system sensitivity.
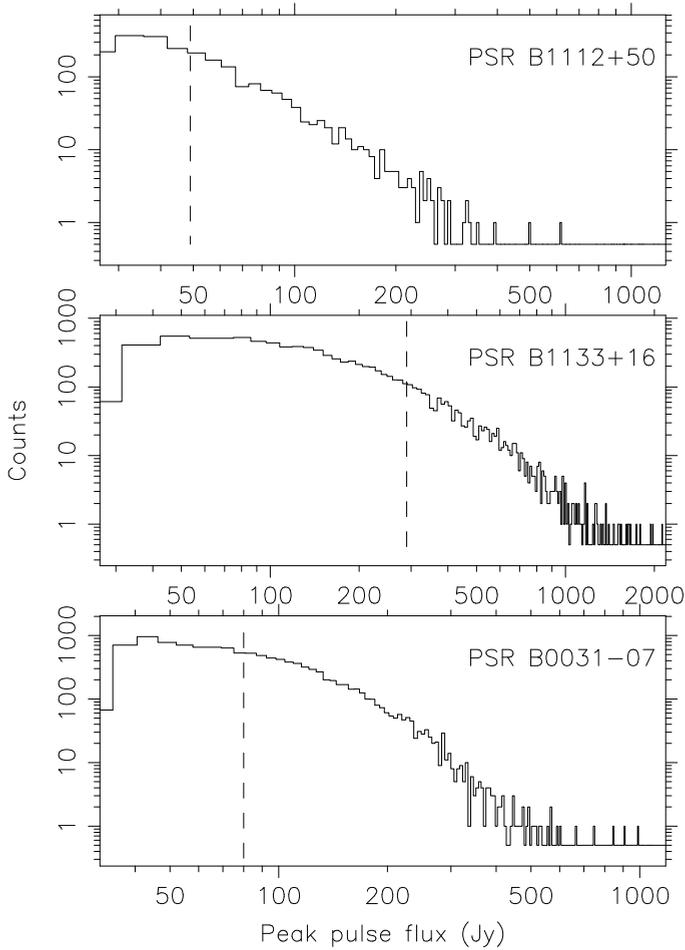
Figure 4.6: Plot of the peak flux distribution of the single pulses for the three pulsars. The dashed line shows $10 \times S_{av,peak}$ for each pulsar.

4.6.3   PSR B0031−07

Kuzmin & Ershov (2004) reported giant pulses from PSR B0031−07. Our observations reveal that the bright and spiky pulses do not satisfy the $10\langle E \rangle$ criterion but are easily greater than $10 \times S_{av,peak}$, as seen in Figures 4.4 and 4.6. Figure 4.4 also reveals the emission of bright pulses on the leading edge of the average pulse profile. The work of Ershov & Kuzmin (2005) (see their Table 1) suggests that the bright pulses in this pulsar have a steep spectral index. We also draw the reader's attention to Figure 4 of Kuzmin & Ershov (2004), where they report the detection of "double giants" in this pulsar at 40 and 111 MHz. Such pulses were dectected in our observations, as seen on the right most panel of Figure 4.3. These bright

subpulses with two distinct peaks show structure spanning a few milliseconds implying that they are not microstructure in the emission. As with PSR B1133+16, the presence of a turn over in the pulsar energy distribution $\sim 1.5\langle E \rangle$ indicates the presence of null emission.

4.7 Microstructure

Several single pulses from both PSR B1133+16 and B0031−07 show pulse structures considerably narrower than the width of the average pulsed emission. The presence of pulses with microstrucure was evident when several thousand pulses were examined in the process of cleaning RFI from the data. To quantify the microstructure, the autocorrelation function (ACF) (Cordes et al. 1990) of the single pulses and their averages were computed. The discrete ACF is defined by,

$$R(\tau) = \sum_{t=0}^{nbin} I(t).I(t+\tau) \tag{4.4}$$

where $I(t)$ is the intensity of the pulsar. Figure 4.7 shows $R(\tau)$ for a single pulse and the averaged ACF of several pulses.

For PSR B1112+50, the single pulses were quite narrow, devoid of any feature that can be recognized as microstructure. Therefore, this pulsar is not considered anymore in this section. The separation between the two main emission components is clearly seen for B1133+16 as the feature at correlation lag ~ 30 ms, which is $\sim 9°$ in pulse longitude. The ACF for the pulse shown in the top most panel shows a periodicity of the microstructure (the local maxima near correlation lag 5 ms in the middle panel of Figure 4.7). It is known that PSR B1133+16 shows structure $\sim 8\mu s$ and a characteristic intensity fluctuation on the order of $\sim 575 – 663\,\mu s$ in the 111–196 MHz range (Hankins 1972). We note that our final resolution of $580\,\mu s$ is not sufficient to resolve narrower structures or permit the estimation of persistent quasi periodic intensity variations in the averaged ACF.

In the case of PSR B0031−07, single pulses show narrow bursty features. However, the single pulse ACF in the right middle panel of Figure 4.7 shows no characteristic variations implying that the pulse consists of non-periodic microstructure. Such nonperiodic features were also found in PSR B0950+08 (Lange et al. 1998). The average subpulse separation is seen in the averaged ACFs. This is visible as the local maxima $\sim 55\ ms$ for PSR B0031−07 and expressed in pulse longitude this is $20°$ which is also the value of P_2 found in §4.8. For the average ACF's displayed in the lower most panels of Figure 4.7, the pulses chosen are detected simultaneously in the two bands. The slight shift of local maxima to the left cannot be measured at a large significance, and indicates the subpulse separation decreases with frequency as can be seen by comparing the subpulse properties at 328 and 1380 MHz in Weltevrede et al. (2006a) and Weltevrede et al. (2007). The slight break at ~ 10 ms in the ACF of the single pulse is the width of microstructure in the pulsar. The reason for the lack of a prominent characteristic timescale in the microstrucure of PSR B0031−07 may be due to our coarse time resolution.
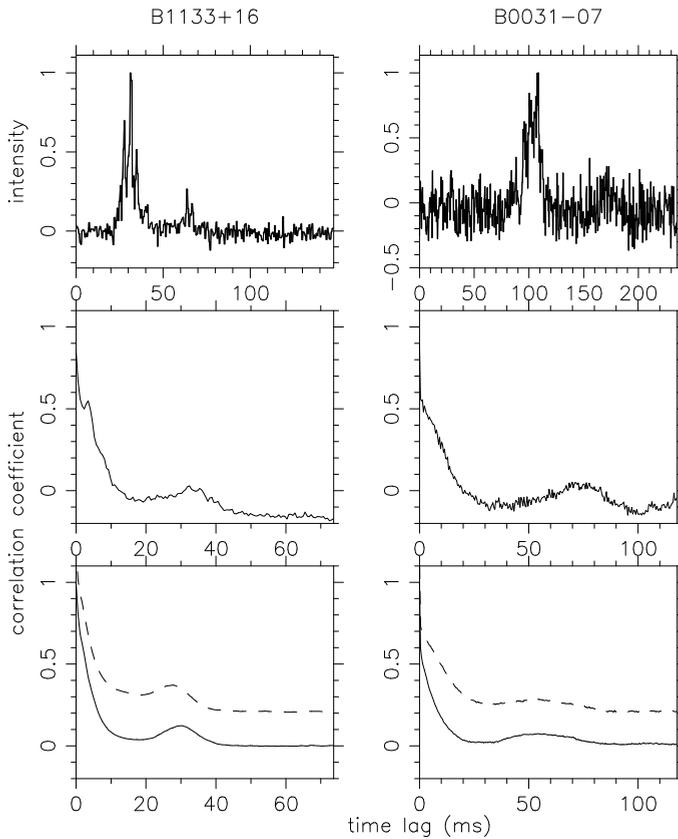
Figure 4.7: Intensity autocorrelation functions (ACF) of pulses with structure for two pulsars. The top most panels display example pulses. The autocorrelations displayed in the middle panel correspond to the pulses above them. The lower most panels display the averaged ACFs for 120 and 132 pulses for PSRs B0031−07 and B1133+16 respectively. The averaged ACF's for two bands centred at 116.75 MHz and 173.25 MHz (dashed line) are shown.

4.8   Fluctuation Spectra

Since the three pulsars under discussion show bright and bursty emission, it is natural to expect considerable pulse to pulse variation. In some pulsars (eg. PSRs B0809+74, B1944+17) the presence of drifting and persistent microstructure were noticed leading Cordes et al. (1990) to suggest that these two phenomena are correlated. Moreover, PSRs B1133+16 and B0031−07 show drifting subpulses at other frequencies. To ascertain the drifting behaviour at these frequencies, we undertook sub-pulse drift analysis.

In order to perform the analysis presented in this section, the pulse stacks were subjected to pulse drift analysis based on the following methods: Longitude-Resolved Modulation In-

dex (LRMI), Longitude-Resolved Fluctuation Spectrum (LRFS) and Two-Dimensional Fluctuation Spectrum (2DFS) (Edwards & Stappers 2002; Weltevrede et al. 2006a). The Sliding Two-Dimensional Fluctuation Spectrum (S2DFS) was also computed to identify the onset of the various drift modes (Serylak et. al, 2009, submitted). The resulting plots from the LRMI, LRFS and 2DFS analysis are shown in Figure 4.8. In this plot, only LRMI values that are detected with a significance of more than 6σ are shown (top panel; Figure 4.8). In the LRFS and 2DFS plots, the presence of drifting subpulses result in regions of enhanced brightness called "features" . The vertical drift rate P_3 and the horizontal separation P_2 of the subpulses are measured as the centroid of a rectangular region in the 2DFS containing the features (Eq. 6; Weltevrede et al. 2006a). The sign of P_2 denotes the direction of the drift, i.e. whether subpulses drift towards the leading (negative) or trailing (positive) edge of the pulsar's average profile respectively. In what follows the S2DFS analysis results are discussed only for PSR B0031−07. The analysis of PSRs B1133+16 and B1112+50 using the S2DFS technique showed results comparable to those obtained from the 2DFS method alone.

The results presented in this section are for the 2.5 MHz band centred at 156 MHz, as in the previous section. In the RFI cleaning procedure discussed in §4.3.1, less than 2% of the pulses were replaced by zero, and therefore the effect is considered small enough to be neglected. The drift analysis was performed on all eight bands, and the results presented here are representative of the other bands. Within the 115–180 MHz range, there are no noteworthy changes in drift features. The modulation index was also in general consistent with the results found in the band reported here but are higher than the values reported in high frequency studies (see Table 4.4).

Pulsar	P_3	P_2	m		
	$[P_0]$	[deg]	21cm	92cm	192cm
B1112+50	6 ± 3	5^{+4}_{-2}	1.5	2.1	3.5
B1133+16[a]	30 ± 5	–	1.4	0.8	2.2
	34^{+5}_{-3}	–			
B0031−07[b]	$12.2^{+0.2}_{-0.1}$	-21^{+2}_{-1}	1.2	1.4	3.1
	6.7 ± 0.1	$-21.6^{+0.5}_{-0.2}$			

[a] Values presented for the leading and trailing component.

[b] Values presented for the drift mode "A" and "B".

Table 4.4: The results from the drift analysis for the three pulsars. Vertical and horizontal separations of the subpulses are listed in columns 2 and 3 respectively. The modulation indices, m at three different wavelengths are shown in last three columns. The 1400 MHz values in column 4 are from Weltevrede et al. (2006a), 328 MHz values in column 5 are Weltevrede et al. (2007), while the results in the last column are from this work.
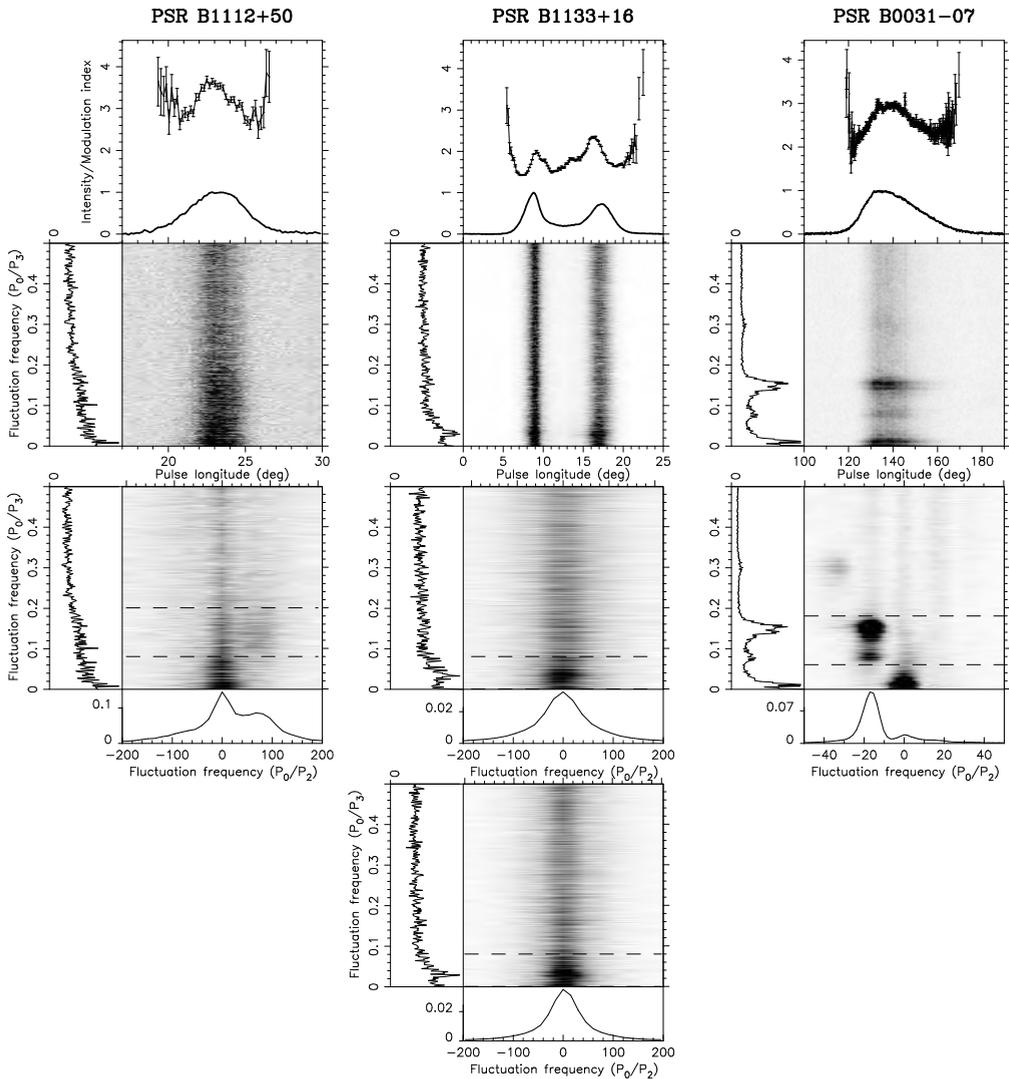
Figure 4.8: Plots of the fluctuation analysis for the PSRs B1112+50, B1133+16, and B0031−07. The average pulse profile, and the Longitude-Resolved Modulation Index (LRMI) are shown in the top most panels. The panels directly below the average pulse profile display the Longitude Resolved Fluctuation Spectrum (LRFS). The Two-Dimensional Fluctuation Spectra (2DFS) are shown in the third and fourth rows. For PSR B1133+16, the 2DFS plots are shown separately corresponding to the two components of the average pulse profile. The panels on the left and bottom of the LRFS and 2DFS images contains the vertically and horizontally integrated spectra respectively.

4.8.1   PSR B1112+50

This pulsar shows a broad, non-specific vertical drift feature as seen in the panels on the left in Figure 4.8. Wright et al. (1986) reported the presence of three different drift modes in this pulsar; the dominant mode in the trailing part of the average pulse profile showed a periodicity of $P_3 \sim 6P_0$. At 328 MHz Weltevrede et al. (2007) report $P_2 = 40^{-10}_{+20}$ degrees and $P_3 = 9 \pm 5P_0$. We detect $P_2 = 5^{+4}_{-2}$ degrees and subpulse modulation of $P_3 = 6 \pm 3P_0$. We also note increased power in the entire range of P_3 centered around $P_0/P_2 = 0$. While the P_3 found here is consistent to values reported elsewhere within the errors, the discrepancy between the P_2 results reported by Weltevrede et al. (2007) and ours can be explained by the higher S/N ratio of individual pulses in our observations. This results in a more prominent feature in the spectrum and less convolution with the increased power in the entire range of P_3 centered around $P_0/P_2 = 0$.

It is possible that only the prominent drift mode active at 1412 MHz (mode 2 of Wright et al. (1986)), is also active at this frequency. The indication comes for this from the similarity in the average profile at our frequency with the average profile computed from 193 pulses containing drift mode 2 in Wright et al. (1986). In their work, the profile computed from 176 pulses in mode 1 displays a prominent double peak. From the LRMI plot, the modulation index $m \sim 3.5$ is quite high at this frequency. Combined with the values reported elsewhere (see Table 4.4), this indicates that the pulse-to-pulse intensity variations increase with decreasing frequency. This again suggests that the large amplitude pulses are more common in this pulsar at lower sky frequencies. The LRFS shows an excess near $P_0/P_3 \sim 0$ which is due to the large nulling fraction, $\sim 60\%$ in the emission of this pulsar (Ritchings 1976) as can be also seen in Figure 4.5. However, this is only indicative of the presence of nulling which has some contribution from the zeros introduced by the RFI cleaning procedure, and these plots cannot be used to measure the pulsar's nulling fraction.

4.8.2   PSR B1133+16

The results of the analysis presented here confirms the presence of the long-period feature $P_3 \sim 30$ at this frequency as was reported at frequencies greater than 300 MHz (Weltevrede et al. 2006a; Herfindal & Rankin 2007). In Figure 4.8 (middle panel) the horizontal component of the drift feature, P_2 is very weak and is consistent with no ordered horizontal separation of the subpulses. We note that the feature near $P_0/P_3 = 0.18$ is present in both components of the pulse profile, while there is significant modulation present in the bridge emission region as seen in the LRMI plot. For the leading component we find $P_3 = 30 \pm 5P_0$ while for the trailing, $P_3 = 34^{+5}_{-3}P_0$. Apart from the aforementioned P_3 feature, the LRFS shows the non-ordered feature that modulates the emission throughout the entire stretch of the analysed pulse sequence. This is also evident from the elevated baseline of the collapsed spectra seen in the side panels. The excess power seen near $P_0/P_3 = 0$ is due to the combination of null emission and the pulses replaced by zeros in the process of cleaning RFI, though as in PSR B1112+50 this cannot be measured reliably from this analysis.

4.8.3   PSR B0031−07

The three different drift modes in this pulsar were first reported by Huguenin et al. (1970), two of which are clearly visible in our analysis (Figure 4.8, right-hand panel). The very low frequency feature at $P_0/P_3 \sim 0.02$ is due to the nulls present in the pulse stack which comes from the combination of null emission and the nulls introduced by RFI cleaning procedure. We detect this feature in all the eight observed bands. The feature seen at $P_0/P_3 = 0.15$ denotes drift mode "B" which is very prominent and therefore introduces aliasing that appears as the feature seen at $P_0/P_3 = 0.3$ cpp. The other feature seen at $P_0/P_3 = 0.08$ is the drift mode "A" and it appears regularly in the pulse stack. The drift mode "C" is not seen in the 2DFS spectrum. We have used the S2DFS method in order to analyse the occurrence rate of different drift modes. While modes "A" and "B" were clearly dectected in the S2DFS output, mode "C" remained undetected. The mode "C" has a low occurance rate and is active only for ~2.6% of the observation time at 327 MHz (Vivekanand & Joshi 1997). Similarly, Smits et al. (2005) detect this mode marginally at 328 MHz but not at 4.85 GHz, indicating a steeper spectral index for the drift mode. Therefore, other than susceptiblity to RFI and lower sensitivity, it is unclear why this mode is not detected at these frequencies.

4.9   Discussion

The long observations reported in this chapter provide good sensitivity to persistent weak features in the average emission of the pulsars. We were thus able to test the hypothesis of interpulse emission in PSR B1112+50 suggested in the work of Wright et al. (1986) at 1400 MHz. Based on the outer gap emission model then proposed, these authors suggest observations at low sky frequencies to detect the inter pulse, as the model predicted large fanbeams. Our deep exposures at low sky frequencies show no evidence for inter pulse emission with an upper limit of 3.5 mJy at 156 MHz (see Figure 4.1) and this is < 0.6% of the main pulse peak flux. The non-dection of an interpulse in this pulsar is not very surprising given that only ~1.5% of the 1847 known pulsars possess an interpulse emission component (Weltevrede & Johnston 2008). Assuming that the neutron star has a dipolar magnetic field, this suggests that PSR B1112+50 is not an orthogonal rotator and its alternate magnetic pole never sweeps across our line of sight. Polarimetric observations of the pulsar might show the inclination of the magnetic and rotational axis.

The spectral indicies found in this study indicate a turn over in the 115–180 MHz range. Michel (1978) modelled the pulsar emission as consisting of a coherent part and an incoherent synchrotron component. This model further predicts a spectral index of −8/3 and a spectral turn over below 100 MHz based on the finite energy of the injected particles, and the radiation is dominated by incoherent emission mechanisms. However, this contrasts with the presence of bright pulses and clear single pulses near the putative turnover frequency which suggests that the radiation is still of a coherent nature. In the simulations by Gil & Kijak (1992) based on the model that the pulsar radiation is a result of emission cones, it is seen that the estimated intensity is very sensitive to the viewing geometry. If the radiation orginates higher in the magnetosphere (as at low sky frequencies), it is possible that the viewing geometry

changes quite rapidly. This in turn can give rise to the observed pulse flux near the spectral turn over resulting in spectra that does not vary smoothly. Detailed polarization studies at these frequencies can be used to test if the observed frequency dependence of the pulse flux has its orgins in the viewing geometry, although the pulse shape is quite stable. In summary, past studies have been inconclusive on the value of spectral index for PSRs B1133+16 and B0031−07 at low sky frequencies. The results presented in this work can be interpreted as evidence of the presence of a turn over in the 115-180 MHz range for PSR B1133+16. These results also indicate that for PSRs B0031−07 and B1112+50, the spectra has already turned over implying that the maximum intensity of these two pulsars may be at $\nu > 180$ MHz.

As pointed out by other authors, the discrepancies in pulsar DMs stem from the difficulty in aligning multi frequency pulse profiles and the choice of a fiducial point in the average profile (Hobbs et al. 2004; Ahuja et al. 2007). The narrow bright pulses at low sky frequencies in the pulsars studied in this work have permitted a very accurate estimation of the DM. We note that scatter broadening of the emitted pulses can limit the accuracy of the DMs estimated by other methods and that of ours. This can be another source of the DM discrepancies. Owing to the broad band nature of the pulsar emission mechanism, we cannot rule out the claim that some pulsars may have a slightly different DM in different parts of the frequency spectrum (Kardashev et al. 1982). Simultaneous broad-band observations with the existing instruments and LOFAR can address these issues effectively.

Based on their widths and large intensities, the bright pulses in our study show some similarities with the normal giant pulses suggesting similar emission mechanisms. Sources of classical giant pulses display a phase correlation of the giant pulses with the high energy non-thermal X-Ray emission as in the Crab pulsar (Lundgren et al. 1995), PSR B1937+21 (Cusumano et al. 2003) and in other millsecond pulsars (Knight et al. 2006b,a). However these are energetic pulsars with large values of B_{LC}. It is known the PSR B1133+16 shows X-ray emission (Kargaltsev et al. 2006), which the authors claim to contain both thermal and non-thermal components. With their coarse time resolution of 3.2 s and low photon counts, these workers were unable to extract the pulse profile at X-ray. However, the non-thermal high energy emission could be related to the bright pulses observed in our work. For PSRs B1112+50 and B0031−07, a deep search in the archival X-Ray data might reveal any correlation that might exist. The double bright pulses reported here and by Kuzmin & Ershov (2004) points to the presence of a global magnetospheric phenomena, despite the different physical locations of the emitting regions. It could be that drifting occasionally brings these two regions into our line of sight resulting in the double pulses. Detailed analysis of such double pulses will provide insights into the phenomena that might be active over the whole magnetosphere.

In the pulsar models forwarded by Ruderman & Sutherland (1975), the radio waves are emitted tangential to the diverging magnetic field lines by the relativistic electron–positron pairs. In this model, the width of the observed average profile is then defined by the last open magnetic field lines. Further, the model predicts that the emitted radio frequencies ν follows a $\nu \propto r^{-3/2}$ relation, where r is the radial distance from centre of the star. This leads to the lower frequencies being emitted higher up in the magnetosphere than the high frequency radio waves, giving rise to a radius-to-frequency mapping (RFM). Our observations

show a decrease in the component separation in the average pulse profile of PSR B1133+16 with frequency and this scales as $v^{-0.3}$. After correcting for the residual DM smearing, the retardation and abberation time delays predicted by the RFM model can be measured from the 116 and 173 MHz average profiles. Using a method similar to Cordes (1978), we find a lower limit of 5.6×10^5 m for the height of 116 MHz radio emission. Depending on the methods used, previously measured emission heights were $< 10^{5.0}$–$10^{5.8}$m and $< 10^{4.7}$–$10^{5.8}$m for the radio emission in the 40–1400 MHz range (Cordes 1978; Matese & Whitmire 1980). The upper limit in these works corresponds to the 40 MHz radiation emitted at radius $r < 10^{5.8} = 6.3 \times 10^5$m. Therefore, the derived emission radius of 5.6×10^5 m for the 116 MHz radiation is consistent with the former results. For the other two pulsars, a reduction in the profile width is visible in Figure 4.1. The lack of a reliable fiducial point in the average profiles of these two pulsars hampers robust estimation of the retardation and abberation time delays, and hence estimation of emission heights.

The drift analysis revealed the large modulation index in all three pulsars at this frequency and they in fact approach that of the Crab pulsar ($m = 5$ to 8) as found by Weltevrede et al. (2006a) and Weltevrede et al. (2007) at 1380 and 382 MHz, respectively. Combined with the values in their work, the modulation index of the pulsars considered here increases with decreasing frequency indicating the prevalence of bright and spiky emission. From their observations in 341–4850 MHz range, Kramer et al. (2003) reported giant pulses in PSR B1133+16 at 4850 MHz, with a majority of them occuring at the phase of the leading component of the average emission profile. They also report individual pulses at 1412 MHz clearly distinct from noise, but less than 10 times the average pulse. Furthermore, these pulses were contemporaneous to the giant pulse emission at 4850 MHz. If the bright pulses we detect are related to those found at 4850 MHz, then this raises the question of why the mechanism responsible for the bright pulses is not active at 1412 MHz. A possible reason for this could be an unusual spectral behaviour of these bright pulses. Alternatively, the average emission could have a greater contribution from the normal pulses at 1.4 GHz than at 4850 MHz or at 116 MHz. Simultaneous observation spanning even wider frequencies than Kramer et al. (2003) could help resolve this issue.

It is interesting to note that the slopes in the edges of the average emission profiles as seen in PSRs B1112+50 and B0031−07 are indicative of the sub-pulse drifting and the direction of the dominant drift mode. These pulsars were also identified as drifters by Weltevrede et al. (2007). From their work, it can also be seen that several pulsars exhibiting coherent drifting show that one of the leading or trailing edges of the average emission profiles is steeper than the other (e.g B2012+51, B2310+42, B2016+28 etc.).

The preference of the bright pulse emission to occur at the phase conicident with the peak in the average emission profile is a feature common to all pulsars in this study. This argues that these pulses are preferentially emitted further away from the last open magnetic line in the magnetosphere, which contrasts with pulsars like PSR B1937+21 (Kinkhabwala & Thorsett 2000). The bright pulses in B0031−07 are more frequent and bright at even lower sky frequencies when we compare our results in the 115–180 MHz range with those found by Ershov & Kuzmin (2005) at 40 MHz. This is also valid for the other two pulsars studied here – bright pulses are more common in these pulsars at lower frequencies. This finding

contrasts with the models of Petrova (2004) in which the bright and narrow giant pulses at high frequencies were explained by inverse Compton scattering of low frequency radio photons. Simultaneous multi wavelength radio observations might help resolve this issue.

4.10 Conclusions

The main conclusion that can be drawn from the pulse energy distributions for PSRs B1133+16 and B0031−07 is that they show a power-law like form in the frequency range observed here. PSR B1112+50 shows a pulse energy distribution with a somewhat steeper power law and several pulses with energy $\geq 10\langle E \rangle$. Even though the pulses detected are much narrower than the average pulse profile, these characteristics alone do not qualify these pulsars as giant pulse emitters in the classical sense. However, the single pulse analysis in these pulsars do reveal the large modulation indicies, suggesting that they are similar to the "spiky" emission as in the in the low frequency observations of B0656+14 (Weltevrede et al. 2006c). Extending this argument further, this emission may be related to the RRAT-like emissions (Weltevrede et al. 2006b).

In this work, the spectrum of three pulsars in the 115–180 MHz range were derived and PSR B1133+16 shows a spectral break in this range, while the spectra of PSRs B1112+50 and B0031−07 show that the spectra peaks at frequencies greater than 180 MHz. From our detections of narrow and bright pulses, we reported DM changes for PSRs B1112+50 and B1133+16 and no change in the DM of PSR B0031−07. We detect microstrucure in PSRs B1133+16 and B0031−07, however with our sensitivity we are not able to measure the characteristic intensity variation timescales. In the drift analysis of the single pulses in PSR B0031−07, two of the three drift modes were detected. The modulation indices computed from the pulse stacks of all three pulsars show values larger than those at higher frequencies. This shows the presence of strong pulse to pulse intensity variations and probably arises from the combination of dritfing subpulses and the single bright pulses. While the issue of whether these pulsars emit giant pulses is not conclusive, it is clear that the nature of emission changes considerably as one moves to lower radio frequencies.

4.11 Acknowledgements